Performance of photosensors in high rate environment for gas Cherenkov

Chao Peng[a], Junqi Xie[a,*], Sylvester Joosten[a], Zein-Eddine Meziani[a], Alexandre Camsonne[b], Mark Jones[b], Edward Kaczanowicz[c], Melanie Rehfuss[c], Nikolaos Sparveris[c], Michael Paolone[d], Michael Foley[e], Michael Minot[e], Mark Popecki[e]

[a]*Argonne National Laboratory, 9700 S Cass Ave., Lemont, IL 60439, USA*
[b]*Thomas Jefferson National Accelerator Facility, 12000 Jefferson Ave., Newport News, VA 23606, USA*
[c]*Department of Physics, Temple University, Philadelphia, PA 19122, USA*
[d]*Department of Physics, New Mexico State University, Las Cruces, NM 88003, USA*
[e]*Incom, Inc., 294 Southbridge Rd., Charlton, MA 01507, USA*
**Corresponding author. E-mail address: jxie@anl.gov (J. Xie).*

Abstract

The upcoming SoLID experiment at Jefferson Lab will push the envelope on luminosity for a large-acceptance detector, requiring the use of a light-gas Cherenkov detector for trigger-level event selection. Due to the high luminosity environment, the single-photon background rate in this Cherenkov is expected to be extremely high at the photon sensor. Thus, it is essential to validate the planned photosensors and readout electronics to determine the limits of these sensors and mitigate the risk of failure of the trigger-level event selection. We report the design of a small prototype telescopic Cherenkov device and a set of early studies in a high-rate environment in Hall C at Jefferson Lab. Commercially available multi-anode photomultipliers (MaPMT) and low-cost large-area picosecond photodetectors (LAPPD) were tested with the JLab FADC250 modules for the data acquisition to assess their performance in such an environment. The experiment results show that both a MaPMT array and an internal stripline LAPPD could detect the Cherenkov signals and separate single-electron events and pair production events. A GEANT4 simulation confirms the experimental performance of the prototype results through direct comparison. With higher quantum efficiency, the MaPMT array provided a better separation of the single-electron events and pair production events than the internal stripline LAPPD. The experiment also demonstrated that the MaPMT array with a summed readout of 16 pixels per MaPMT, the LAPPD with internal stripline readout, and the FADC250 modules performed successfully at a single-photon rate up to 60 kHz/cm^2.

Keywords:

High luminosity experiment, gas Cherenkov counter, photomultiplier, high rate environment

1. Introduction

In the 12 GeV era of Jefferson Laboratory, some nuclear physics experiments will operate at the luminosity frontier [1-2]. In each case, the unprecedented luminosity requirement imposes new challenges on detector technology, trigger design, and data acquisition. For example, the pillars experiments in the Solenoidal Large Intensity Device (SoLID) require operation at a luminosity of 10^{37} - 10^{39} $cm^{-2}\cdot s^{-1}$ [2]. In these experiments, a high threshold light-gas Cherenkov detector (LGC) will be crucial to create efficient triggers that identify electrons and reject pions.

Traditional Cherenkov threshold counters use a gas radiator (e.g., N_2, CO_2, CF_4, and C_4F_{10}) at atmospheric pressure and serve as one of the main detectors for electron-pion separation. The radiator provides a cone of Cherenkov light for electrons passing through the medium while leaving no response for pions with energies below the radiator's energy threshold. Single readout dynode type photomultipliers (PMT) are used to detect the Cherenkov photon cone. The crucial challenge for gas Cherenkov detectors in high luminosity experiments is the exceedingly high rate of background photons. The single-photon background rate inside these detectors, caused mainly by π^0 decay, is estimated up to 4 MHz per 5×5 cm^2 area. This background rate makes a traditional approach of using standard 3- or 5-inch quartz-glass dynode-type photomultipliers impossible due to their sensitivity to a magnetic field and difficulty to be tiled to cover a large uniform sensitive area. Furthermore, placing large traditional photomultipliers, together with the required shielding inside these spectrometers, is also not feasible due to the limited available space. These issues may be solved by using magnetic field resilient and high granularity photosensors, such as multi-anode photomultiplier tubes (MaPMTs) [3-6] and microchannel plate photomultipliers (MCP-PMTs) [7-10].

Currently, 64-pixel MaPMTs are commercially available from Hamamatsu [11]. They are sensitive to the spatial distribution of intensity across their surface and are used or proposed to replace traditional tube PMTs in many experimental devices [12-15]. Compared to standard quartz-glass PMTs, MaPMTs have a square shape and high granularity (pixel size of 6×6 mm^2); thus, they can be tiled to cover a large uniform detection plane. They can also be coated with p-Terphenyl wavelength shifter [16] to provide high detection efficiency in the UV spectrum. However, one major drawback of MaPMTs is their relatively lower magnetic field tolerance, requiring bulky full-array mu-metal shielding in a magnetic field above 50 Gauss for a high-efficiency operation [17]. The additional shielding not only complicates the detector design but also increases the final detector cost. MCP-PMTs are built upon an advanced technology that employs microchannel plates to replace conventional discrete dynodes for electron signal amplification [10]. Commercial MCP-PMTs have been shown to have superior timing and position resolution, high granularity,

as well as high magnetic field tolerance [18, 19]. These advantages make the MCP-PMTs an advanced photosensor candidate to achieve simple system design and efficient trigger selection, but they are generally too expensive to be used widely. A novel, recently commercialized MCP-PMT, the Large Area Picosecond Photo-Detector (LAPPD) [20-22], provides a promising cost-effective MCP-PMT for Cherenkov photon counting and imaging applications. The LAPPDs use low-cost micro-channel plates activated by applying resistive and secondary emissive layers on a large-area glass capillary substrate through the atomic layer deposition (ALD) technique. The cost of LAPPD is expected to be at least an order of magnitude lower per active area than that of traditional MCP-PMTs. For a given sensor coverage area, this projected cost reaches a price range competitive to that of using MaPMTs, and promoting the LAPPD as a candidate photosensor for future Cherenkov counters.

The high granularity of MaPMTs and MCP-PMTs allows the Cherenkov cone to illuminate multiple active areas, generating spatially distributed signals. A simple coincidence requirement of at least two nearby signal channels fire could drastically reduce the accidental single-photon background. Undoubtedly, this novel application of the MaPMTs and MCP-PMTs in a harsh environment with unprecedented background requires extensive testing to guide design decisions and provide input for realistic simulations. In this paper, we report the design of a small Cherenkov telescope, along with the photosensor evaluation experiments performed at the Thomas Jefferson National Accelerator Facility (TJNAF, a.k.a Jefferson Lab or JLab). The small detector was installed in a realistic "open" high rate environment in JLab Hall C, and the test data were taken parasitically to the on-going fixed-target experiments. Both commercially available MaPMTs and LAPPD were tested as photosensors. Cherenkov photon signals from good electron tracks were observed and investigated. The detection performance of MaPMTs and LAPPD in this high rate environment was studied for their possible application in future generic gas Cherenkov counters.

2. Small Cherenkov telescope design

A small Cherenkov telescope, as shown in Figure 1, was designed to generate and collect the Cherenkov photons. The device consists of four components: (1) the main detector tank, (2) the flat reflective mirror, (3) the gas pressure monitor system, and (4) the photosensor.

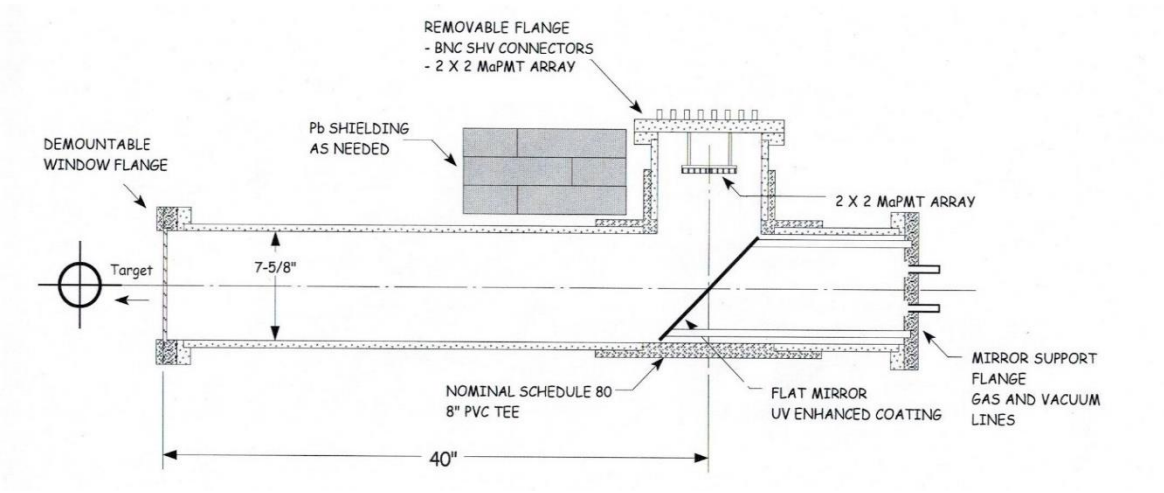

Figure 1. Schematic of the small Cherenkov telescope for Cherenkov photons generation and detection.

The main detector tank was constructed out of standard schedule-80 PVC pipes with an inner diameter of 7-5/8 inches. A tee-socket was used to connect the three individual PVC pipes into a telescope shape. The 40-inch long pipe faced the target during the experiment to allow scattered electrons to pass through the gas radiator and generate Cherenkov photons. The radiator was kept just above atmospheric pressure by an entrance and exit windows made out of aluminum of 0.003-inch thickness. A flat mirror (Spectra Thin Films, Hauppauge, NY) coated with a thin aluminum film for enhanced ultraviolet (UV) light reflection was placed in the center of the tee-socket at an angle of 45^{o} with respect to the center of the main pipe. The mirror role was to reflect the Cherenkov photons by 90^{o} to land on the surface of the photosensors, which were mounted on the side port of the tee-socket and protected from radiation damage by lead blocks. The interior of the entire system was coated with light-absorbing paper to minimize internal reflection. A 370 nm light-emitting device (LED) was installed near the entrance window for calibration and checking purposes.

A gas system from the SANE Cherenkov counter [23] was re-purposed and installed on the small Cherenkov telescope to regulate the gas pressure slightly above atmospheric pressure. Operating at atmospheric pressure helped simplify the mechanical design and minimized the windows thicknesses. Both nitrogen or carbon dioxide (N_2 or CO_2) were used as the radiator medium in this system. The small Cherenkov telescope was flushed in several cycles to ensure a high gas purity before stabilizing it at atmospheric pressure.

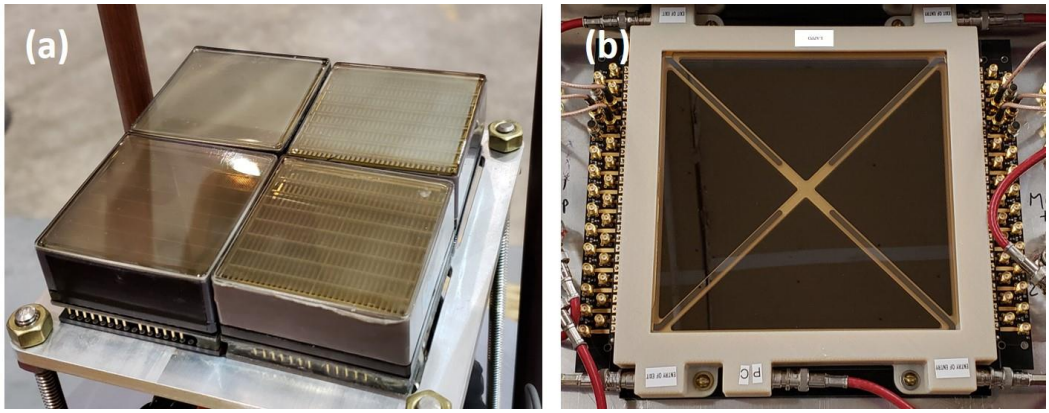

Figure 2. Images of the (a) 10x10 cm^2 p-Therphenyl coated MaPMT array, and (b) 20x20 cm^2 LAPPD.

An array of 2 × 2 Hamamatsu MaPMTs (2 × H8500 and 2 × H12700) was tiled together to provide a photosensor area of roughly 10x10 cm^2 to detect the Cherenkov photons. Each MaPMT comprises an 8 × 8 array of 5.80 mm × 5.80 mm pixels. For the SoLID light gas Cherenkov counter application, it is unnecessary to have such a small pixel size, so we summed every 16 pixels of a quadrant for each MaPMT into one readout channel to reduce the number of readout channels for cost savings and for providing a generous number of photoelectrons per channel. In total, we had 16 channels for the 2 × 2 array of Hamamatsu MaPMTs, i.e., 4 channels per MaPMT. Figure 2 (a) shows an image of the 2 × 2 MaPMT array. All four MaPMTs were coated with a p-terphenyl wavelength shifter to enhance the UV photon response through absorption in the UV region and re-emission at lower wavelengths matching the maximum quantum efficiency of the uncoated MaPMTs [16]. A low-cost internal stripline LAPPD (LAPPD #41) was provided by Incom, Inc. to characterize its performance in a high-rate environment. It features an active area close to 20 × 20 cm^2 and has 28 stripline readout [21]. Pixelized LAPPDs are still under development and were not yet commercially available when our experimental test was conducted. The performance of a pixelized device will be characterized in a future measurement. Figure 2 (b) shows an image of the internal stripline LAPPD. Due to its large size, a dark adaptor box was designed and built to accommodate the LAPPD. The received LAPPD was specially made with UV transparent fused silica entrance window, so no p-terphenyl wavelength shifter coating was applied. The geometry and performance parameters of the Hamamatsu MaPMT H8500, H12700, and Incom LAPPD received for our experiment are listed in table 1.

Table 1. Geometry and performance parameters of photosensors to be investigated

	Hamamatsu 8500	**Hamamatsu 12700**	**Incom internal stripline LAPPD**
PMT type	MaPMT	MaPMT	MCP-PMT
Device type	5cm × 5cm	5cm × 5cm	20cm × 20cm

Active area	10cm x 5cm	10cm x 5cm	20cm x 20 xm
Readout type	Pixel	Pixel	Stripline
Entrance window material	UV glass	UV glass	Fused silica
Wavelength shifter coating	Yes	Yes	No
Response wavelength range	185 – 650 nm	185 – 650 nm	220 – 700 nm
Quantum efficiency	28%	35%	7.3% (max 11%)
Operation high voltage	950 V	950 V	2550 V (MCP = 975 V)
Gain	10^6	10^6	4×10^6

3. Experimental setup

The small Cherenkov telescope was installed in Hall C at JLab, as shown in Figure 3. The setup was 4.8 meters away from the target scattering chamber and mounted to level with the beamline and target. Its entrance window was facing the target at an angle of 68^o with respect to the beam direction. The distance between the target chamber and the entrance window was 4.8 meters. The distance and angle were chosen to have a moderate rate background environment; it was also limited by space and safety concerns. Lead blocks were placed next to the photosensors to protect them from direct radiation damage caused by the target generated background.

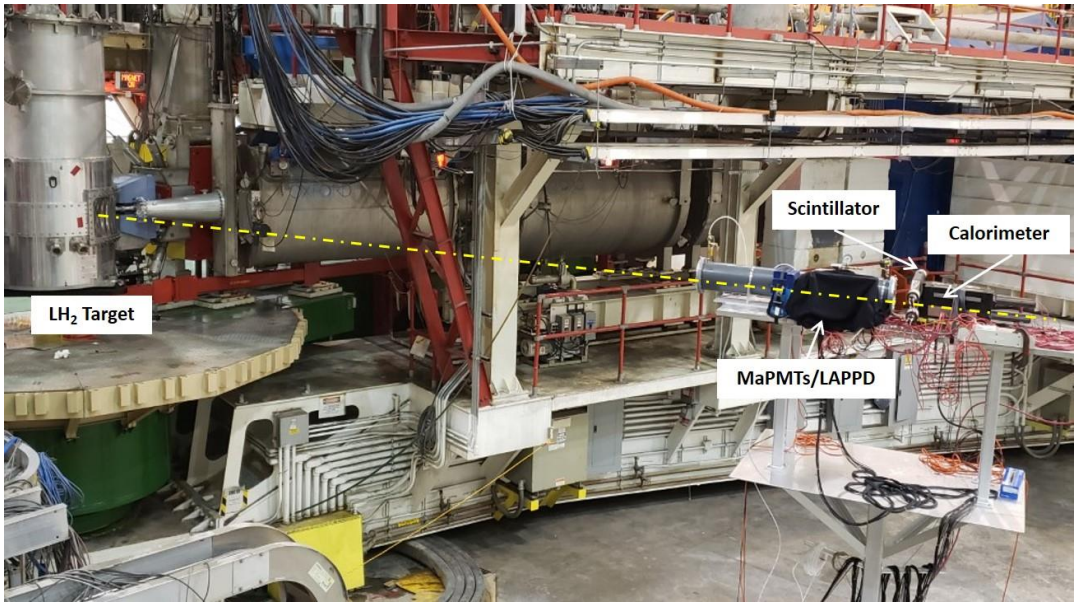

Figure 3. Small Cherenkov telescope installed on a platform in Hall C. The setup was lifted to the level of the beamline, 4.8 meters away from the liquid hydrogen target, and with the entrance window facing the target chamber. Scintillator bars and calorimeter blocks were used at the back for the trigger. Photosensors were protected from radiation damage with lead blocks.

The external trigger was provided by the scintillator bars and the calorimeter blocks, which were placed behind the exit window of the small Cherenkov telescope. Four calorimeter blocks, previously used for the HERA-B calorimeter outer section cells [24], were stacked together to ensure the full coverage of the exit window area. For trigger purposes, each calorimeter block had one readout channel. The calorimeter threshold was set to ~500 mV (at a high level) to ensure that only significant signals triggered the detector readout. The trigger and signals from the scintillator, calorimeter, and photosensors were all fanned-out and sent to two custom-made F250 flash Analog-to-Digital Converters (FADC250) [25] for data acquisition.

During the experiment, we used an 8.1 GeV electron beam, impinging a liquid H_2 target. When a high energy particle (mainly scattered electron) traveled through the small Cherenkov telescope, which was filled with CO_2 at atmospheric pressure, a cone of Cherenkov photons was emitted along the particle path. The Cherenkov photons were then reflected onto the photosensors by the flat mirror. Simultaneously, the particle continued traveling through the mirror and generated trigger signals in the scintillator and calorimeter, initiating the data acquisition.

4. Results and Discussion

4.1 Electronics rate estimation in the experiment

Since we expected the single-photon background to contribute a majority of the rate, we estimated each channel's electronics rate by counting the number of triggered events with MaPMTs as the photosensor. Figure 4 shows the estimated electronics rate for each channel. In our experimental conditions, except for one MaPMT, each quadrant event's rate was about 400 kHz, which is ~ 1.5 MHz rate per MaPMT, or 60 kHz/cm^2.

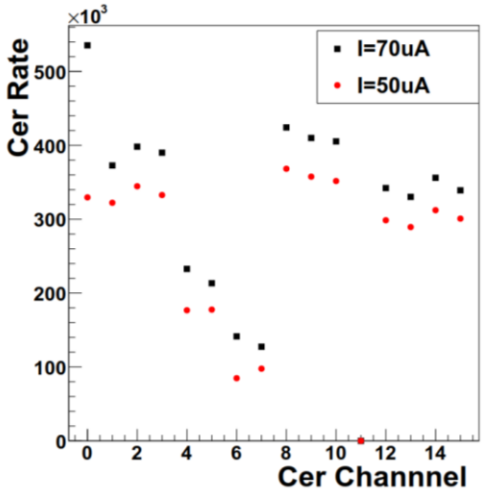

Figure 4. Estimation of electronics rate for each channel.

4.2 Hamamatsu MaPMT array response

The scintillators were saturated during our experiment due to the very high background rate, so only calorimeter signals were considered for the trigger during the data analysis. The timing difference between the signal and calorimeter trigger showed a Gaussian distribution with a sigma of 1~2 ns for all channels. Figure 5 shows the signal amplitude distribution of each channel within a 3σ timing cut. Channel 11 data was not recorded due to a signal wire connection issue. It can be seen that a significant single photoelectron background dominates the raw MaPMT signals. Signal correlation analysis is necessary to select good events from the background. Meanwhile, signals with large amplitudes were concentrated on channel 8~15, indicating that the small Cherenkov telescope was not optimally aligned. The Cherenkov photon cone appears shifted to the lower side of the MaPMT array.

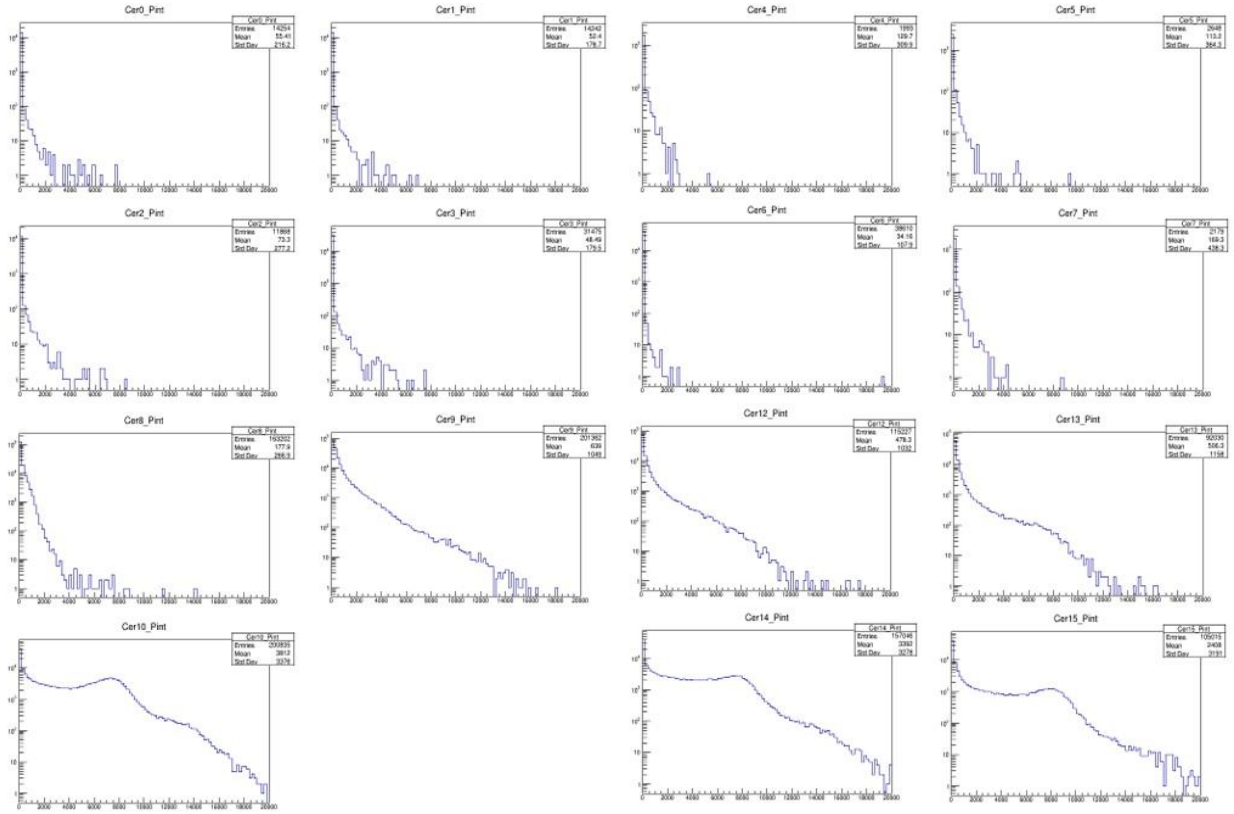

Figure 5. Signal amplitude distribution of each channel within a 3σ timing cut. Channel 11 data was not recorded due to its wire connection issue. Notice the high event rate at a small amplitude in each channel due to the high background rate.

With a perfect alignment to the line-of-sight of the target center, the Cherenkov photon cone generated by an electron along the axis of the tank is expected to cover the central area of the sensors with an outer diameter of 7.7 cm and an inner diameter of 1.2 cm, indicated by the shadow area in Figure 6 (a). Figure 6 (b) illustrated a possible Cherenkov cone positional shift to demonstrate how the misalignment affected the Cherenkov photon collection. Given that the alignment adjustment was not possible due to a limited and

opportunistic access to the experimental hall, unfortunately this issue could not be addressed at the time of the measurement. A future experiment with a broader area photosensor coverage and a more suitable alignment which will mitigates this issue is discussed in section 5.

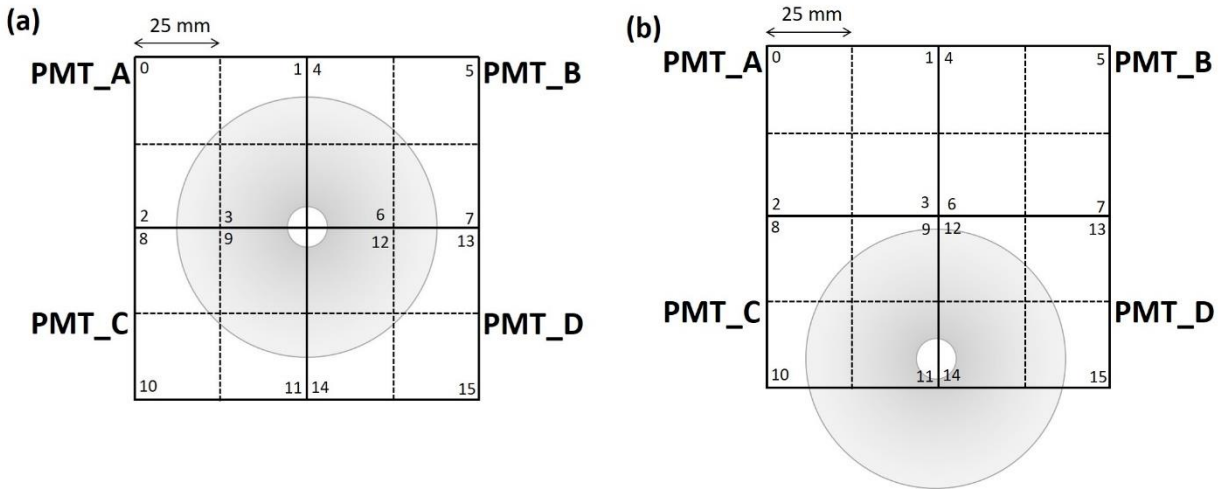

Figure 6. The electronic configuration of the 2 × 2 Hamamatsu MaPMTs array in small Cherenkov telescope. The shadow indicates the Cherenkov photon cone in (a) a perfect alignment condition, and (b) a possible position shift due to misalignment. Cherenkov photons were collected by the PMT C and D only.

Pixel correlation and high threshold selection were applied in our event-by-event data analysis to reduce the background events. We extracted signal waveforms of all channels from the raw data and noticed some signal waveforms with negative values, which are most likely due to a crosstalk between neighbouring channels in the MaPMT response. After removing the crosstalk signals, the distribution of the number of fired channels with a signal threshold at 100 ADC units was obtained and shown in Figure 7 (a). The firing count for each event ranges from 0 to 8 but we were concerned that in the events with low fired channel counts the background may still not be fully rejected. For this reason, events with high fired channel counts were chosen for further analysis to ensure a selection of Cherenkov photon events with the lowest background level. Figure 7 (b) shows the ADC spectra of the Cherenkov signal summed over all the channels with a firing count of 6. Two prominent peaks can be identified in the resulting distribution, with the smaller peak at about twice the ADC value of the prominent peak. The latter represents the single electron Cherenkov events, while the smaller peak corresponds to the possible high energy photons conversion to electron-positron pair originating at the aluminum telescope entrance window. A two-gaussian fit was performed to extract the mean (μ) and standard deviation (σ) of the prominent event peak, and the mean number of detected photoelectrons (N_{pe}) was estimated following the equation below [26]:

$$N_{pe} = \frac{\mu^2}{\sigma^2}$$

The calculation gave an experimental N_{pe} of 14, half of what was expected from the theoretical prediction (N_{pe} ~30). This large difference was later understood and found to be due to the mirror misalignment, as discussed in the GEANT4 simulation section below. In fact, the MaPMTs photosensors array collected only about half of the generated Cherenkov photons.

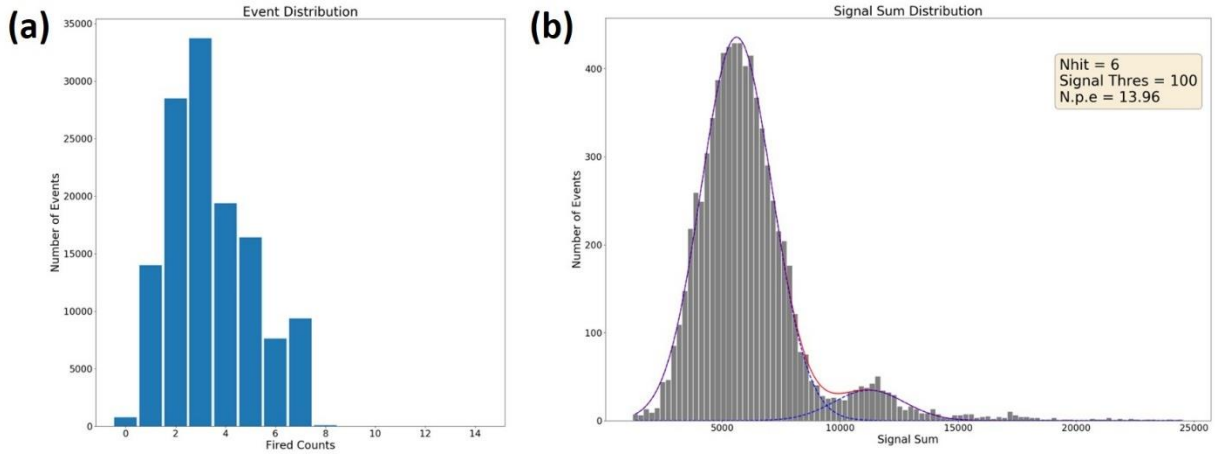

Figure 7. (a) Distribution of event channel firing count after crosstalk signal removal and with a signal sum threshold at 100 ADC value. (b) ADC spectra of the Cherenkov signal integrated sum for events with channel firing count of 6. Notice the pair production events at twice the signal sum of the prominent single events.

4.3 GEANT4 Simulation

A detailed simulation was developed with the GEANT4 simulation toolkit [27] to explain the observed experimental results. It simulates the Cherenkov photons' generation process and path while high energy particles from the target, such as electrons and photons find their way through the prototype detector. The refractivity of the radiator, the experimentally determined mirror reflectivity, and the quantum efficiency of the MaPMTs were all considered in the simulation. Figure 8 shows events visualizations from the simulation which include the geometrical setup starting from the target location, the entrance aluminum window of to the detector, the radiator volume and the photosensor array of 4 MaPMTs. In this visualization, incoming electrons (red traces) generate multiple optical photons (green traces) through the Cherenkov process in the CO_2 gas. Most of the optical photons are reflected by the mirror and then get detected by the photosensor. In the simulation, electrons and photons are generated at the liquid hydrogen target cell at energies from 3 to 8 GeV. The angular distribution of the incident electrons follows the cross-section of electron scattering off a structure-less proton, namely the Mott cross section. Particles detected by the calorimeter having a total energy deposited greater than 0.5 GeV will trigger the detector in the simulation. As a result, the accepted phase-space of these incident particles is shown in Figure 9. It was found that with an additional mirror tilt angle of 15^o the output from simulation describes the data best, as shown in Figure

10. With such a mirror misalignment correction, the simulation results agree well with our experiment results and strongly support our data analysis findings.

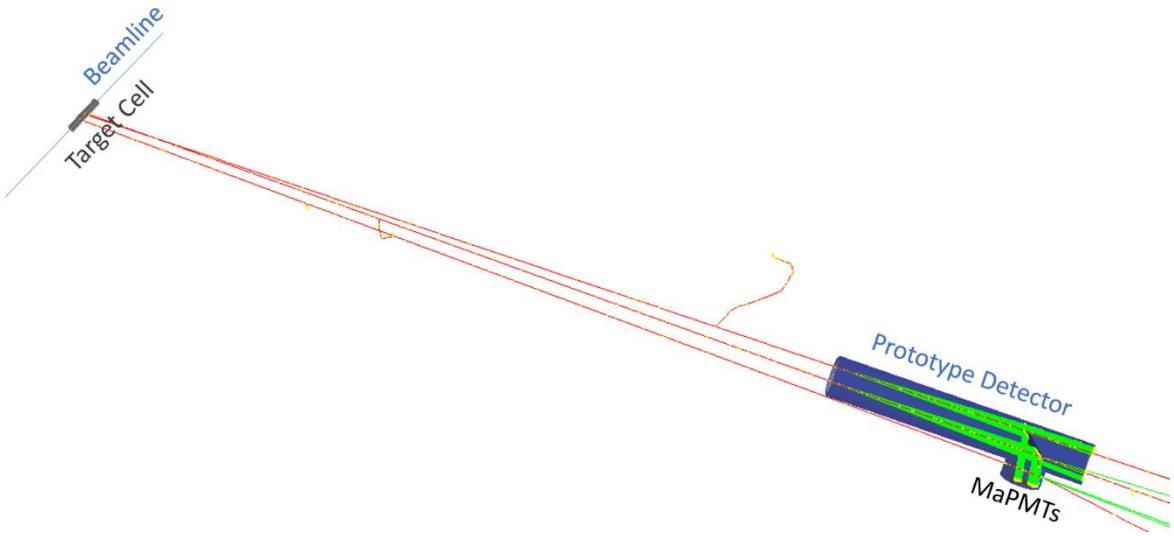

Figure 8. Geometrical setup and the visualization of a few events in the simulation. The red traces represent the incoming electrons, and green traces show the optical photons generated via the Cherenkov process in the CO_2 gas. Most of the optical photons are reflected by the mirror and are detected by the MaPMT array.

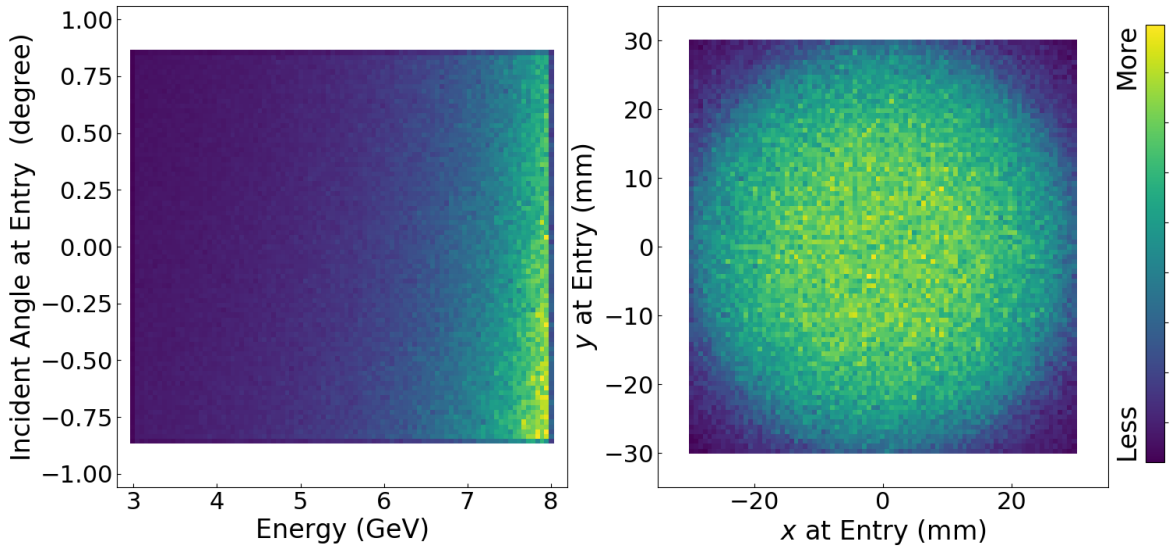

Figure 9. The phase space of incident events that triggered the detector. Angles and positions are with respect to the geometric center of the longitudinal cylindric tank.

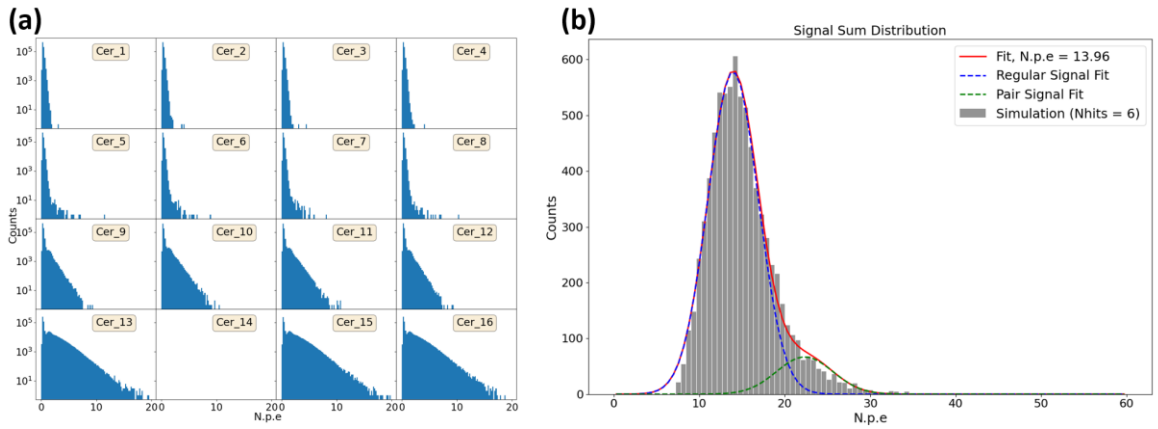

Figure 10. Simulation results with an additional 15° tilt of the mirror. (a) Signal amplitude distribution of each channel from the simulation. One channel is turned off to be consistent with the experimental data (see Figure). (b) Sum of signals requiring the total firing count of 6 channels.

4.4 LAPPD with stripline readout

The 20 × 20 cm^2 LAPPD was accommodated in a dark box attached to the Cherenkov tank for photon detection. The stripline readout and electronic channel configuration are shown in Figure 11 (a). The Cherenkov photon cone projection on the LAPPD, with a mirror misalignment similar to that of the MaPMTs array test, is indicated by the circular light shadow area. In this case, however, the large LAPPD active area allowed the collection of all generated Cherenkov photons even with the misaligned mirror.

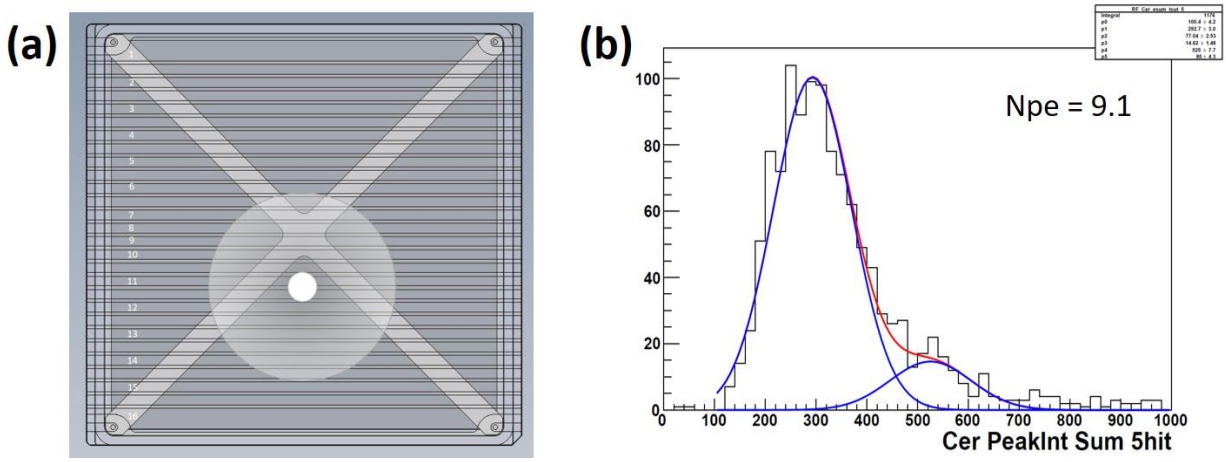

Figure 11. (a) Stripline readout and electronic channel configuration of the LAPPD in the small Cherenkov telescope. The "X" indicates the position of the X cross spacer in the device. (b) ADC spectra of the Cherenkov signal integral sum for events with channel firing count of 5. Notice the pair production events at twice the ADC unit of the prominent single events.

The same event-by-event data analysis method, including 3σ timing cut, pixel correlation, and high threshold selection, was applied in the LAPPD data. The ADC spectra of the Cherenkov signal integral sum

for events with channel a firing count of 5 is shown in Figure 11 (b). The prominent single events and the following pair production events are separated in the histogram. The center value of the pair production events is precisely twice that of the single events. The experimental number of photoelectrons of 9.1 (N_{pe} = 9.1) was obtained from the two gaussian fittings of the distribution. The experimental N_{pe} value agrees with the expected N_{pe} of 10.8 from the theoretical calculation for this LAPPD used in our setup. The small N_{pe} is expected because of the known low QE (~7.3%) of this LAPPD.

Comparing the ADC spectra using the LAPPD as photosensor to that using the MaPMT array, one note that the LAPPD exhibits a slightly worse separation of the single events and pair-production events than the MaPMT. The worse performance of this LAPPD is due to the known lower QE when compared to that of the MaPMTs. With pixelized readout and higher QE, we expect the LAPPD to exhibit a much better separation. The spatial information of the signals can further be utilized to perform pattern recognition, a feature important for Ring Imaging Cherenkov detector, for example.

5. Summary and future work

We reported the design of a small telescopic Cherenkov device and a set of early prototype studies in an open high-rate environment at Jefferson Lab. Commercially available MaPMTs and a low-cost internal stripline LAPPD were tested using a small Cherenkov telescope to assess their performance in a high rate background environment. Both MaPMTs and LAPPD were able to operate in such an environment, detect the Cherenkov signals and separate single-electron events and pair production events. At this time, MaPMTs show a better separation than the LAPPD used thanks to their higher QE and pixelated readout and despite a slight mirror misalignment that reduced the photon collection by a factor of two. Large area LAPPD collected all Cherenkov photons by displayed an overall smaller detection efficiency. In both cases a GEANT 4 computer simulation helped us discover the misalignment of the mirror and fully understand the performance of each detector. Our experiment confirms that the MaPMTs array, internal stripline LAPPD, and the FADC electronics could handle the estimated rate of 60 kHz/cm^2 needed high background rate experiments,

The reported experiment is a preliminary performance validation of photosensors and electronics where we gained a significant experience, with modest resources, from this opportunistic but limited test. A Cherenkov prototype with a full scale MaPMT array and pixelated LAPPD would be desirable in the future. The full-scale Cherenkov prototype must have a higher tolerance to misalignment, and collect all Cherenkov photons. Higher QE, pixelated LAPPD with capacitively coupled readout, under development at Incom, would become available for testing, to evaluate the possibility of pixelated LAPPD as an advanced

photosensor for the SoLID Cherenkov counters. Meanwhile, with mature technology, the LAPPD performance has improved considerably since the production of the LAPPD used in our preliminary test. Our next step is to perform a dedicated test with extreme luminosity conditions expected in the SoLID Parity Violation Deep Inelastic Experiment [28].

Acknowledgement

Argonne National Laboratory's work was supported by the US Department of Energy, Office of Science, Office of Nuclear Physics, under contract DE-AC02-06CH11357. Part of the work was supported by Laboratory Directed Research and Development (LDRD) funding from Argonne National Laboratory, provided by the Director, Office of Science, of the US Department of Energy under contract DE-AC02-06CH11357. The work at Temple University is supported by the US Department of Energy award DE-SC0016577. Incom's work is supported by the U. S. Department of Energy, Office of Science, Office of Basic Energy Sciences, Offices of High Energy Physics and Nuclear Physics under DOE contracts: DE-SC0015267, DE-SC0017929, DE-SC0018778, and DE-SC0019821. This material is based upon work supported by the U.S. Department of Energy, Office of Science, Office of Nuclear Physics under contract DE-AC05-06OR23177.

References

[1] J.P. Chen et al., A Whitepaper on SoLID (Solenoidal Large Intensity Device) (2014). arXiv:1409.7741

[2] The SoLID Collaboration, SoLID (Solenoidal Large Intensity Device) Updated Preliminary Conceptual Design Report, November 2019. < https://hallaweb.jlab.org/12GeV/SoLID/ >

[3] F. Takasaki et al., Development of multianode photomultiplier tube, Nucl. Instrum. Methods Phys. Res. A 260 (1987) 447. https://doi.org/10.1016/0168-9002(87)90115-X

[4] M. Calvi et al., Characterization of a Hamamatsu R7600 multi-anode photomultiplier tube with single photon signals, JINST 8 (2013) P02012. https://doi.org/10.1088/1748-0221/8/02/P02012

[5] L. Cadamuro et al., Characterization of the Hamamatsu R11265-103-M64 multi-anode photomultiplier tube, JINST 9 (2014) P06021. https://doi.org/10.1088/1748-0221/9/06/P06021

[6] M. Calvi et al., Characterization of the Hamamatsu H12700A-03 and R12699-03 multi-anode photomultiplier tubes, JINST 10 (2015) P09021. https://doi.org/10.1088/1748-0221/10/09/P09021

[7] J.L. Wiza, Microchannel plate detectors, Nucl. Instrum. Methods Phys. Res. A 162 (1979) 587. https://doi.org/10.1016/0029-554X(79)90734-1

[8] M. Akatsu et al., MCP-PMT timing property for single photons, Nucl. Instrum. Methods Phys. Res. A 528 (2004) 763. https://doi.org/10.1016/j.nima.2004.04.207

[9] S. Korpar et.al., Timing and crosstalk properties of BURLE multi-channel MCP PMTs, 528 (2008) 169. https://doi.org/10.1016/j.nima.2008.07.022

[10] T. Gys, Micro-channel plates and vacuum detectors, Nucl. Instrum. Methods Phys. Res. A 787 (2015) 254. https://doi.org/10.1016/j.nima.2014.12.044

[11] Hamamatsu Photonics < https://www.hamamatsu.com/us/en/index.html >

[12] P. Križan et al., Tests of a multianode PMT for the HERA-B RICH, Nucl. Instrum. Methods Phys. Res. A 394 (1997) 27. https://doi.org/10.1016/S0168-9002(97)84164-2

[13] E Albrecht et al., A prototype RICH detector using multi-anode photo multiplier tubes and hybrid photo-diodes, Nucl. Instrum. Methods Phys. Res. A 456 (2001) 233. https://doi.org/10.1016/S0168-9002(00)00581-7

[14] E. Aguiló et al., Test of multi-anode photomultiplier tubes for the LHCb scintillator pad detector, Nucl. Instrum. Methods Phys. Res. A 538 (2005) 255. https://doi.org/10.1016/j.nima.2004.08.116

[15] M. Contalbrigo et al., Single photon detection with the multi-anode CLAS12 RICH detector, Nucl. Instrum. Methods Phys. Res. A 952 (2020) 162123. https://doi.org/10.1016/j.nima.2019.04.077

[16] S. Joosten et al., Enhanced UV light detection using a p-terphenyl wavelength shifter, Nucl. Instrum. Methods Phys. Res. A 870 (2017) 110. https://doi.org/10.1016/j.nima.2017.06.050

[17] S. Eisenhardt et al., Characterization and magnetic field properties of multianode photomultiplier tubes, Nucl. Instrum. Methods Phys. Res. A 766 (2014) 167. https://doi.org/10.1016/j.nima.2014.05.036

[18] Y. Ilieva et al., MCP-PMT studies at the High-B test facility at Jefferson Lab, JINST **11** (2016) C03061. https://doi.org/10.1088/1748-0221/11/03/C03061

[19] A. Lehmann et al., Recent progress with microchannel-plate PMTs, Nucl. Instrum. Methods Phys. Res. A 952 (2020) 161821. https://doi.org/10.1016/j.nima.2019.01.047

[20] M.J. Minot et al., Pilot production & commercialization of LAPPD^{TM}, Nucl. Instrum. Methods Phys. Res. A 787 (2015) 78. https://doi.org/10.1016/j.nima.2014.11.025

[21] M.J. Minot et al., Large Area Picosecond Photodetector (LAPPD^{TM}) - Pilot production and development status, Nucl. Instrum. Methods Phys. Res. A 936 (2019) 527. https://doi.org/10.1016/j.nima.2018.11.137

[22] A.V. Lyashenko et al., Performance of Large Area Picosecond Photo-Detectors (LAPPD^{TM}), Nucl. Instrum. Methods Phys. Res. A 958 (2020) 162834. https://doi.org/10.1016/j.nima.2019.162834

[23] W.R. Armstrong et al., A threshold gas Cherenkov detector for the Spin Asymmetries of the Nucleon Experiment, Nucl. Instrum. Methods Phys. Res. A 804 (2015) 118. https://doi.org/10.1016/j.nima.2015.09.050

[24] G. Avoni et al., The electromagnetic calorimeter of the HERA-B experiment, Nucl. Instrum. Methods Phys. Res. A 461 (2001) 332. https://doi.org/10.1016/S0168-9002(00)01237-7

[25] H. Dong et al., Integrated Tests of a High Speed VXS Switch Card and 250 MSPS Flash ADCs, 2007 IEEE Nuclear Science Symposium Conference Record, Honolulu, HI (2007) 831-833. https://doi.org/10.1109/NSSMIC.2007.4436457

[26] LS Peak, and P.Soler, Assessment of the photoelectron number for photomultipliers under conditions of low light intensities, Nucl. Instrum. Methods Phys. Res. A 301 (1991) 341. https://doi.org/10.1016/0168-9002(91)90477-8

[27] S. Agostinelli et al., Geant4—a simulation toolkit, Nucl. Instrum. Methods Phys. Res. A 506 (2003) 250. https://doi.org/10.1016/S0168-9002(03)01368-8

[28] P. Bosted et al., Precision Measurement of Parity-violation in Deep Inelastic Scattering Over a Broad Kinematic Range, JLab Proposal PR12-09-012, December 2008. < http://hallaweb.jlab.org/collab/PAC/PAC34/PR-09-012-pvdis.pdf/ >